

Vacancy-induced ferromagnetism in ZnO probed by spin-polarized positron annihilation spectroscopy

Masaki Maekawa, Hiroshi Abe, Atsumi Miyashita, Seiji Sakai, Shunya Yamamoto, and Atsuo Kawasaki

Citation: *Appl. Phys. Lett.* **110**, 172402 (2017); doi: 10.1063/1.4979696

View online: <http://dx.doi.org/10.1063/1.4979696>

View Table of Contents: <http://aip.scitation.org/toc/apl/110/17>

Published by the [American Institute of Physics](#)

Fearful for the future of science?

Programs and Resources | Publications | Career Resources | Member Societies | About AIP | [Contact Us](#)

Home » Publications

FYI
FOR THE FUTURE OF PHYSICS

on authoritative news and resources

FYI This Week
A newsletter, issued each Monday evening and covers the upcoming week and its features on the physics.

The Week Ahead
Learn about the week's events, research, and more.

Plus: Career Opportunities

Sign up for FREE FYI emails.
AIP American Institute of Physics

FYI Bulletin

Vacancy-induced ferromagnetism in ZnO probed by spin-polarized positron annihilation spectroscopy

Masaki Maekawa, Hiroshi Abe, Atsumi Miyashita, Seiji Sakai, Shunya Yamamoto, and Atsuo Kawasuso

Quantum Beam Science Research Directorate, National Institutes for Quantum and Radiological Science and Technology, 1233 Watanuki, Takasaki, Gunma 370-1292, Japan

(Received 8 December 2016; accepted 18 March 2017; published online 25 April 2017)

We investigated the ferromagnetism of ZnO induced by oxygen implantation by using spin-polarized positron annihilation spectroscopy together with magnetization measurements. The magnetization measurements showed the appearance of ferromagnetism after oxygen implantation and its disappearance during post-implantation annealing at temperatures above 573 K. The Doppler broadening of annihilation radiation (DBAR) spectrum showed asymmetry upon field reversal after oxygen implantation. The obtained differential DBAR spectrum between positive and negative magnetic fields was well-explained with a theoretical calculation considering zinc vacancies. The disappearance of the field-reversal asymmetry of the DBAR spectrum as a result of annealing agreed with the observations of ferromagnetism by magnetization measurements. These results suggest the radiation-induced zinc vacancies to be the source of the observed ferromagnetism of ZnO. *Published by AIP Publishing.*
[\[http://dx.doi.org/10.1063/1.4979696\]](http://dx.doi.org/10.1063/1.4979696)

Discovery of ferromagnetic behavior of a hafnium oxide (HfO₂) thin film in 2004 made an impact, showing that ferromagnetism could be induced by lattice defects even without intentional doping with ferromagnetic elements.¹ Many subsequent investigations demonstrated that such “d⁰ ferromagnetism” is a common feature of metal oxides. Zinc oxide (ZnO), which is a wide-bandgap semiconductor, is one of such metal oxides that shows d⁰ ferromagnetism.² From the coexistence of macroscopic ferromagnetism observed by magnetization measurements and lattice defects detected by X-ray diffraction,³ Hall effect measurement,⁴ electron microscopy,⁵ photoluminescence spectroscopy,^{6–8} X-ray absorption spectroscopy,^{9,10} and positron annihilation spectroscopy,^{11–13} the lattice defects are thought to cause the ferromagnetism. Based on the *ab initio* studies, it has been proposed that zinc vacancies are the likely candidate.^{14–21} The previous positron annihilation studies supported this theoretical prediction. Moreover, zinc vacancies and ferromagnetism have been observed to coexist. This observation, however, is only a circumstantial evidence for zinc vacancy-induced ferromagnetism. To directly determine whether zinc vacancies cause ferromagnetism, the magnetic moments of zinc vacancies need to be detected. To do this, spin-polarized positron annihilation spectroscopy (SP-PAS) could be a uniquely powerful method.

The probability of a positron–electron pair annihilation depends on the total spin (S). For $S=0$, a positron–electron pair immediately annihilates and produces two gamma rays. For $S=1$, most of the electron-positron pairs that do annihilate produce three gamma rays.²² Because the probability of such three-gamma annihilation is only 1/1115 that of two-gamma annihilation, positrons and electrons with antiparallel spins tend to end up pairing, resulting in $S=0$ and two-gamma annihilation. Thus, if both positrons and electrons are spin-polarized, then two-gamma annihilation characteristics, such as the annihilation lifetime, Doppler broadening of annihilation radiation (DBAR), and angular correlation of

annihilation radiation (ACAR), change upon spin reversal and so excess electron spin can be detected. To date, SP-PAS based on ACAR has been used for studying spin-polarized electronic states of ferromagnets. Recently, we demonstrated that the DBAR method and lifetime measurements can also be used for the same purpose.^{23–26} Considering that positrons are preferentially trapped at vacancy defects, magnetic moments associated with vacancy defects may be detected by using the SP-PAS method.²⁷ In this study, we applied the DBAR-based SP-PAS method to the issue of vacancy-induced ferromagnetism in ZnO.

The samples tested were commercial (Optostar Ltd.) hydrothermally grown ZnO single crystals with the dimensions of 10 × 10 × 0.5 mm. To remove residual defects introduced during the crystal growth, all the samples were annealed at 1473 K for 2 h in air.²⁸ Then, the samples were subjected to X-ray diffraction measurements. The width of the 2θ - ω rocking curve was reduced from 0.011° for the unannealed sample to 0.0032° for the annealed sample, indicating improvements in the crystallinity, although native defects would not be removed completely by this heat treatment. Oxygen ions with an energy of 100 keV were implanted into the samples to achieve doses of 10¹² O⁺/cm² to 10¹⁷ O⁺/cm² (flux: 1 μA) at room temperature. The depth of ion implantation was estimated to be 100 nm by using the Stopping and Range of Ions in Matter (SRIM) code.²⁹ After oxygen implantation, the samples were subjected to isochronal annealing below 1473 K for 1 h in air.

Magnetization (M-H) curves were acquired by the superconducting quantum interference device measurements at 100 K. Figure 1(a) shows a schematic of the positron beam apparatus used here. Longitudinally spin-polarized positrons each with a polarization P_+ of 27% and energy of 6 keV were injected into the samples cooled to 15 K. The positron implantation profile is found to overlap the SRIM-predicted vacancy profile (Fig. 1(b)) due to oxygen implantation. The energy spread of the slow positron beam is ~1%,³⁰ and

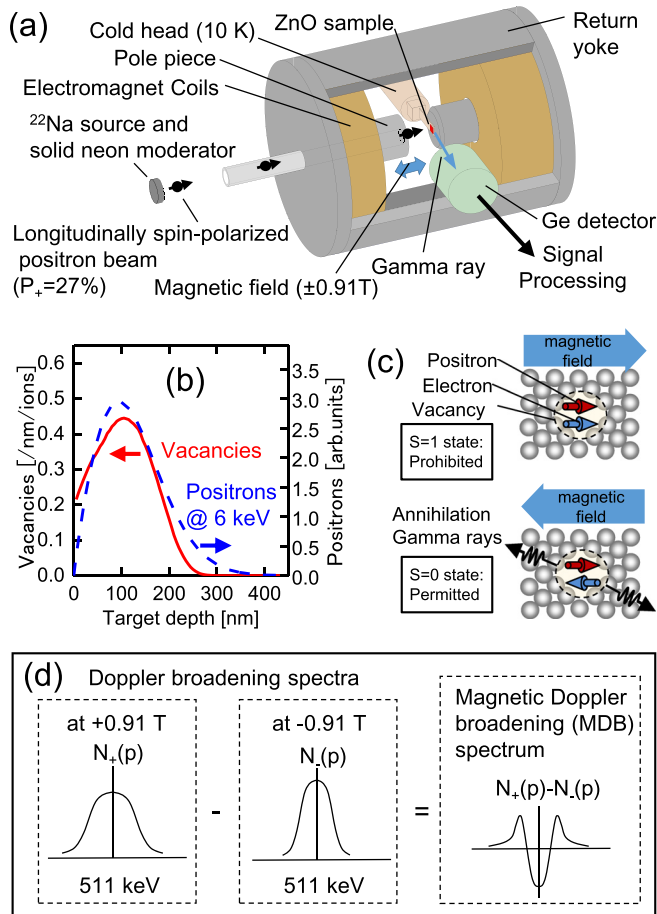


FIG. 1. (a) Schematic of the positron annihilation measurement system. Longitudinally spin-polarized positrons were injected into the sample mounted on the cold stage (15 K) between the electromagnet pole pieces ($\pm 0.91\text{ T}$). Annihilation gamma rays (511 keV) were detected by a Ge detector. (b) Calculated depth distributions of vacancies and positrons. (c) and (d) Schematic representation of the principle of the DBAR-based SP-PAS method. Electron spins are ferromagnetically aligned in the magnetic field. When positron spins and electron spins are parallel* (antiparallel), two-gamma annihilation is prohibited (permitted). Consequently, the shape of the DBAR spectrum undergoes a field reversal, as is also visualized in the MDB spectrum, which shows the difference between the positive and negative fields. *More strictly, $S = 1$ and $m_S = \pm 1$, where m_S is the magnetic quantum number.

hence the influence on the positron implantation profile is almost negligible. The DBAR measurements were taken in magnetic fields of $\pm 0.91\text{ T}$ using a Ge detector with an energy resolution of 1.9 keV at 1.33 MeV .^{31,32} The energy Doppler shift from 511 keV ($=m_0c^2$, where m_0 is the electron rest mass and c is the speed of light) corresponds to an electron momentum of $p = 3.92 \times 10^{-3} m_0c$ per 1 keV . More than 3×10^6 events were accumulated in each spectrum. Backgrounds arising from random coincidence and Compton scattering were subtracted by applying a numerical method.³³ Here, the difference between the DBAR spectrum of the positive field and that of the negative field, $N_+(p) - N_-(p)$, is called the ‘magnetic Doppler broadening (MDB)’ spectrum. A positive (resp. negative) field is defined by the positron polarization and the magnetic field direction being parallel (resp. antiparallel). Figures 1(c) and 1(d) schematically explain the principle of this method. If electron spins at vacancies are made to align parallel or antiparallel to positron spins by changing the field direction, then the probability of a two-gamma annihilation of

positrons with unpaired electrons occurring would be changed. Consequently, the shape of the DBAR spectrum in one field direction may be different from that in the opposite field direction, as easily observed in the MDB spectrum. To evaluate vacancy defects, S and W parameters were also calculated with the energy window of $510.2\text{--}511.8\text{ keV}$ and $514.8\text{--}517.4\text{ keV}$. All the S and W parameters were normalized to that of the unimplanted sample.

To interpret the experimental MDB data, a theoretical calculation was carried out assuming appropriate defect models. The details of the theoretical framework and the calculation were described elsewhere.²⁶ The electron wave functions were obtained by carrying out an ABINIT computation³⁴ with the projector-augmented-wave method.³⁵ For Zn and O atoms, the valence electron configurations were $3s^23p^63d^{10}4s^2$ and $2s^22p^4$, respectively. For the defect structures, the supercell included 32 Zn and 32 O atoms. The lattice constants were fixed to $a = 3.25\text{ \AA}$ and $c = 5.21\text{ \AA}$.³⁶ In the calculation of defect structures, only the gamma point was considered. The lattice relaxations around defects were considered based on the molecular dynamics simulation implemented in the ABINIT code. The cut-off energy of the plane-wave basis set was 60 Ry . The core electron wave function was represented by the Slater function parameterized by Clementi and Roetti.³⁷ A self-consistent positron wave function was calculated based on two-component density functional theory in order to minimize the energy functional. The Boroński–Nieminen enhancement factor was adopted.³⁸ The DBAR spectrum was obtained by double-integrating the momentum density with a Gaussian convolution having a full width at half-maximum of 1.9 keV .

Figure 2(a) shows M-H curves obtained before and after ion implantation. Although weak (background) magnetization

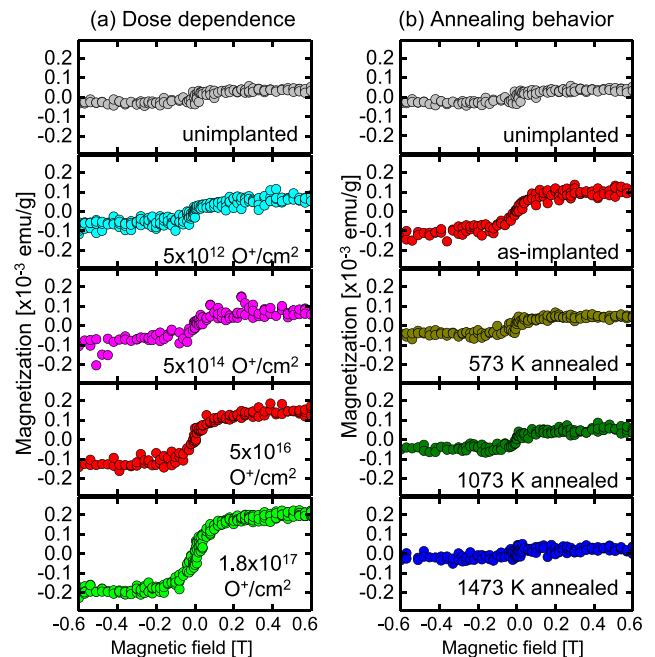


FIG. 2. (a) Irradiation dose dependence and (b) post-annealing temperature dependence of M-H curves for the oxygen-implanted ZnO single crystals measured at a temperature of 100 K. The implantation dose for the annealing behavior experiments was $5 \times 10^{16}\text{ O}^+/\text{cm}^2$. The annealing duration at each temperature was 1 h.

is seen before implantation, an increase in magnetization to a level exceeding the background level is found to be induced by oxygen implantation. The magnetization increase with increasing ion dose appears to saturate above $5 \times 10^{16} \text{ O}^+/\text{cm}^2$. The background magnetization in the unimplanted state arises from the whole region of the sample (which was 0.5 mm thick). This might be due to residual impurities, such as iron, whereas the magnetization induced by oxygen implantation results from the shallow ion depth ($\sim 200 \text{ nm}$). Hence, the net magnetization induced by oxygen implantation should be much greater than that in the unimplanted state. Figure 2(b) shows how annealing influenced the M-H curve obtained for the sample implanted with a dose of $5 \times 10^{16} \text{ O}^+/\text{cm}^2$. After annealing at 573 K, the magnetization is reduced to almost the same level as for the unimplanted state. These results suggest that the ferromagnetism is induced in the ZnO by oxygen implantation and that some defects are the source. The disappearance of magnetization by post-implantation annealing may have been related to the recovery of the defects. The magnetization decreased to 80% from 100 K to room temperature. This suggests that the Curie temperature is higher than room temperature.

Figure 3 shows the S-W plot for the various annealing temperatures together with theoretical values.³⁹ The inset shows S parameters for the unimplanted and as-implanted states as a function of positron incident energy. After the oxygen implantation, S parameters increase at $5 \text{ keV} < E < 15 \text{ keV}$. This S-E profile matches the calculated distributions of vacancies in Fig. 1(b). All subsequent measurements were performed at the energy of 6 keV. (S, W) = (1, 1) corresponds to the unimplanted and bulk states in experiment and calculation. The calculated S and W parameters for the nearest-neighbor divacancy ($V_{\text{Zn}}V_{\text{O}}$) and zinc vacancy (V_{Zn}) are on distinguishable two lines from the bulk state. The experimental S and W parameters are located nearby those calculated for zinc vacancy in the as-implanted state and shifted towards the calculated values for divacancy after

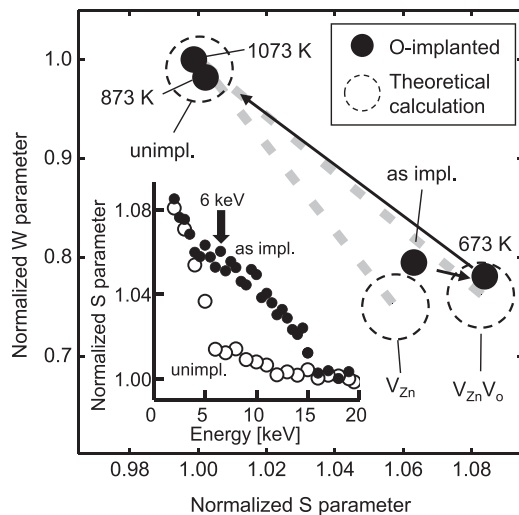


FIG. 3. S-W plot obtained for the oxygen implanted sample at various annealing temperatures. Filled circles show the experiments. Open circles are the calculated values for zinc vacancy (V_{Zn}) and nearest-neighbor divacancy ($V_{\text{Zn}}V_{\text{O}}$). The inset shows S parameters for unimplanted and as-implanted state as a function of positron incident energy.

673 K annealing. At higher annealing temperature, S and W parameters move to the bulk state. These suggest that zinc vacancies disappear around 673 K leaving divacancies (and presumably also higher order vacancy clusters) that are annealed out above 873 K. This behavior is in good agreement with the previous electron beam experiment.⁴⁰ This annealing temperature of zinc vacancies agrees with that of magnetization by superconducting quantum interference device (SQUID). As shown below, the MDB measurements provide further evidence for the zinc vacancy-induced ferromagnetism.

Figure 4(a) shows the MDB spectra at different ion doses. The MDB spectrum of the unimplanted sample is nearly flat. But, after oxygen implantation, the amplitude increase with ion dose tends to saturate above $5 \times 10^{16} \text{ O}^+/\text{cm}^2$. Figure 4(b) shows the annealing behavior of the MDB spectrum obtained for the sample implanted with a dose of $5 \times 10^{16} \text{ O}^+/\text{cm}^2$. The MDB spectrum becomes nearly flat for the annealing carried out at 673 K. The effects of dose and annealing on the MDB spectrum are found to be very similar to their effects on the M-H curve (Fig. 2). A previous study showed positrons to be nearly fully trapped at zinc vacancies in oxygen-implanted ZnO,⁴¹ and other studies showed the contribution of oxygen vacancies to be very small.^{42,43} The change of the DBAR spectrum itself upon oxygen implantation (characterized by the so-called S parameter) indicates the positrons to be trapped by zinc vacancies in the current samples as well. The solid lines shown in Fig. 4(a) (for $5 \times 10^{16} \text{ O}^+/\text{cm}^2$ and $1.8 \times 10^{17} \text{ O}^+/\text{cm}^2$) are theoretical MDB spectra calculated by assuming an electrically neutral zinc vacancy. (The amplitudes here were adjusted by a factor of 0.42 and 0.2 to be comparable to

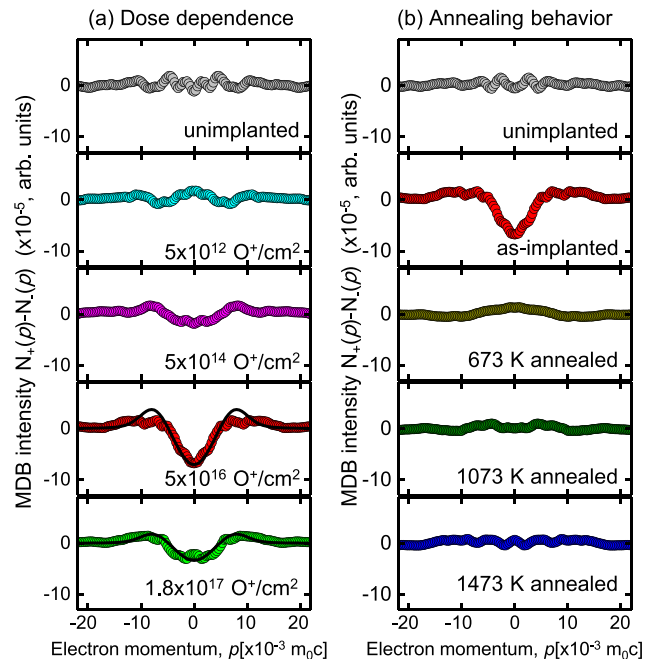


FIG. 4. (a) The irradiation dose dependence and (b) the post-annealing temperature dependence of the magnetic Doppler broadening (MDB) spectrum $[N_+(p) - N_-(p)]$ in an external magnetic fields of $\pm 0.91 \text{ T}$ at 15 K. The solid lines in the $5 \times 10^{16} \text{ O}^+/\text{cm}^2$ and $1.8 \times 10^{17} \text{ O}^+/\text{cm}^2$ panels are MDB spectra calculated using the ABINIT code, which adjusts amplitudes to levels comparable with the experiments. The implantation dose used for the annealing behavior experiments was $5 \times 10^{16} \text{ O}^+/\text{cm}^2$. The annealing duration at each temperature was 1 h.

the corresponding experiments.) The MDB spectra calculated for an oxygen vacancy and nearest-neighbor divacancy are completely flat. An electrically neutral zinc vacancy is in a high spin state with $S = 1$, and hence it possesses a magnetic moment of $2.0 \mu_B$ (μ_B : the Bohr magneton).¹⁹ Such a high spin state is not available for an oxygen vacancy or a nearest-neighbor divacancy. At zinc vacancies, positrons are preferentially annihilated together with oxygen 2p electrons. Due to the momenta of oxygen 2p electrons being higher than those of outer-shell electrons of zinc atoms, the intensity of the MDB spectrum becomes negative at around $p = 0 m_0c$ and positive at around $\pm 7 m_0c$, as shown in Fig. 4(a). A similar shape was observed for the MDB spectrum of iron, which results from its 3d electrons.²³ This similarity results from the similar radial distributions of oxygen 2p electrons and iron 3d electrons.^{18,19}

After zinc vacancies disappear, some secondary defects may be generated. However, the above results show that such defects induce no ferromagnetism. It is reported that ferromagnetism may be induced through the interaction between oxygen vacancies and Mn impurities.⁴⁴ Considering the fact that positrons are rarely trapped by the oxygen vacancies,^{42,43} the present results are hardly attributed to such oxygen vacancy-related defect complexes. Enhancement of the ferromagnetism in Co-doped ZnO by the mediation of Zn-related vacancies is theoretically predicted.⁴⁵ However, the crystal used in this study is not intentionally doped with Co. Even though zinc vacancies couple with impurities, the agreement between experimental MDB spectrum and that calculated for zinc vacancies suggests that those impurities are not located at the vicinity of zinc vacancies.

As shown above, both the magnetization and the amplitude of the MDB spectrum appear to saturate above $5 \times 10^{16} \text{ O}^+/\text{cm}^2$. This observation suggests that the number of zinc vacancies is high enough to induce magnetic interactions between these vacancies. Considering that the amplitudes of the experimentally determined MDB spectra were 20% ~ 40% of those of the corresponding theoretical ones, the effective magnetization per zinc vacancy is estimated to be 0.4–0.8 μ_B . (The estimation of effective magnetization per zinc vacancy from the M-H measurements is somewhat problematic because of uncertainty in estimating the number of zinc vacancies.) Since the zinc vacancies have acceptor levels in the lower half of the band gap and the Fermi levels of the present samples are located in the mid-gap, the charge state of zinc vacancies is probably the mixture of neutral and single negative. The reduced magnetization per zinc vacancy (less than $2.0 \mu_B$) may have resulted from the elimination of the high spin state due to the occupation of the acceptor levels with additional electrons having antiparallel spins.

In conclusion, by using SP-PAS, we have obtained direct evidence for Zn vacancies being responsible for the ferromagnetism in oxygen-implanted ZnO. There are many kinds of materials, including oxides,^{46,47} nitrides,⁴⁸ carbides,⁴⁹ and graphite,⁵⁰ which are anticipated to exhibit d^0 ferromagnetism. SP-PAS should be a useful tool for confirming whether d^0 ferromagnetism is induced by vacancies. Considering the low carrier density and high vacancy density after irradiation, one possible reason of magnetic coupling might be the electron hopping among vacancies.

This work was financially supported by JSPS KAKENHI under Grant Nos. 24310072 and 15K14135.

- ¹M. Venkatesan, C. Fitzgerald, and J. M. D. Coey, *Nature* **430**, 630 (2004).
- ²N. H. Hong, J. Sakai, and V. Bríže, *J. Phys.: Condens. Matter* **19**, 036219 (2007).
- ³N. H. Hong, J. Sakai, N. T. Hung, N. Poirrot, and A. Ruyter, *Phys. Rev. B* **72**, 045336 (2005).
- ⁴Q. Xu, H. Schmidt, S. Zhou, K. Potzger, M. Helm, H. Hchmuth, M. Lorenz, A. Setzer, P. Esquinazi, C. Meinecke, and M. Grundmann, *Appl. Phys. Lett.* **92**, 082508 (2008).
- ⁵P. Zhan, W. Wang, C. Liu, Y. Hu, Z. Li, Z. Zhang, P. Zhang, B. Wang, and X. Cao, *J. Appl. Phys.* **111**, 033501 (2012).
- ⁶G. Z. Xing, Y. H. Lu, Y. F. Tian, J. B. Yi, C. C. Lim, Y. F. Li, G. P. Li, D. D. Wang, B. Yao, J. Ding, Y. P. Feng, and T. Wu, *AIP Adv.* **1**, 022152 (2011).
- ⁷S. Ghosh, G. G. Khan, B. Das, and K. Mandal, *J. Appl. Phys.* **109**, 123927 (2011).
- ⁸S. Ghosh, G. G. Khan, B. Das, and K. Mandal, *EPJ Web Conf.* **40**, 03001 (2013).
- ⁹W. Yan, Z. Sun, Q. Liu, Z. Li, Z. Pan, J. Wang, and S. Wei, *Appl. Phys. Lett.* **91**, 062113 (2007).
- ¹⁰S. B. Singh, Y.-F. Wang, Y.-C. Shao, H.-Y. Lai, S. Hsieh, M. V. Limaye, C.-H. Chuang, H.-C. Hsueh, H. Wang, J.-W. Chiou *et al.*, *Nanoscale* **6**, 9166 (2014).
- ¹¹D. Wang, Z. Q. Chen, D. D. Wang, N. Qi, J. Gong, C. Y. Cao, and Z. Tang, *J. Appl. Phys.* **107**, 023524 (2010).
- ¹²M. Khalid, M. Ziese, A. Setzer, P. Esquinazi, M. Lorenz, H. Hochmuth, M. Grundmann, D. Spemann, T. Butz, G. Brauer, W. Anwand, G. Fischer, W. A. Adeagbo, W. Hergert, and A. Ernst, *Phys. Rev. B* **80**, 035331 (2009).
- ¹³H. Ren, G. Xiang, G. Gu, X. Zhang, W. Wang, P. Zhang, B. Wang, and X. Cao, *J. Nanomater.* **2012**, 295358 (2012).
- ¹⁴W. A. Adeagbo, G. Fischer, A. Ernst, and W. Hergert, *J. Phys.: Condens. Matter* **22**, 436002 (2010).
- ¹⁵Q. Wang, Q. Sun, G. Chen, Y. Kawazoe, and P. Jena, *Phys. Rev. B* **77**, 205411 (2008).
- ¹⁶X. Zuo, S.-D. Yoon, A. Yang, W.-H. Duan, C. Vittoria, and V. G. Harris, *J. Appl. Phys.* **105**, 07C508 (2009).
- ¹⁷D. Kim, J. Yang, and J. Hong, *J. Appl. Phys.* **106**, 013908 (2009).
- ¹⁸P. Dev and P. Zhang, *Phys. Rev. B* **81**, 085207 (2010).
- ¹⁹O. Volnianska and P. Boguslawski, *J. Phys.: Condens. Matter* **22**, 073202 (2010).
- ²⁰O. Volnianska and P. Boguslawski, *Phys. Rev. B* **83**, 205205 (2011).
- ²¹J. Yhun, Z. Zhang, and T. Yin, *Sci. World J.* **2013**, 541496 (2013).
- ²²S. Berko, in *Positron Annihilation*, edited by A. T. Stewart and L. O. Roellig (Academic Press, New York, 1967), p. 72.
- ²³A. Kawasuso, M. Maekawa, Y. Fukaya, A. Yabuuchi, and I. Mochizuki, *Phys. Rev. B* **83**, 100406(R) (2011).
- ²⁴A. Kawasuso, M. Maekawa, Y. Fukaya, A. Yabuuchi, and I. Mochizuki, *Phys. Rev. B* **85**, 024417(6) (2012).
- ²⁵A. Kawasuso, Y. Fukaya, M. Maekawa, I. Mochizuki, and H. Zhang, *J. Phys.: Conf. Ser.* **443**, 012084 (2013).
- ²⁶H. Li, M. Maekawa, A. Kawasuso, and N. Tanimura, *J. Phys.: Condens. Matter* **27**, 246001 (2015).
- ²⁷S. Hagiwara, Y. Suzuki, and K. Watanabe, *Appl. Phys. Express* **9**, 041001 (2016).
- ²⁸Z. Q. Chen, M. Maekawa, A. Kawasuso, S. Sakai, and H. Naramoto, *J. Appl. Phys.* **99**, 093507 (2006).
- ²⁹J. F. Ziegler, J. P. Biersack, and D. Ziegler, *The Stopping and Range of Ions in Matter* (SRIM Company, 2008).
- ³⁰M. Maekawa, K. Wada, Y. Fukaya, A. Kawasuso, I. Mochizuki, T. Shidara, and T. Hyodo, *Eur. Phys. J. D* **68**, 165 (2014).
- ³¹M. Maekawa, H. Zhang, H. Li, Y. Fukaya, and A. Kawasuso, *Jpn. J. Appl. Phys. Conf. Proc.* **2**, 011305 (2014).
- ³²M. Maekawa, Y. Fukaya, H. Zhang, H. Li, and A. Kawasuso, *J. Phys.: Conf. Ser.* **505**, 012033(4) (2014).
- ³³M. Haaks, T. E. M. Staab, and K. Maier, *Nucl. Instrum. Methods, A* **569**, 829 (2006).
- ³⁴X. Gonze, J.-M. Beuken, R. Caracas, F. Detraux, M. Fuchs, G.-M. Rignanesse, L. Sindic, M. Verstraete, G. Zerah, F. Jollet *et al.*, *Comput. Mater. Sci.* **25**, 478 (2002).
- ³⁵P. E. Blöchl, *Phys. Rev. B* **50**, 17953 (1994).
- ³⁶O. Madelung, *Semiconductors Basic Data* (Springer-Verlag, Berlin, 1996), p. 182.

- ³⁷E. Clementi and C. Roetti, *At. Data Nucl. Data Tables* **14**, 177 (1974).
- ³⁸E. Boroński and R. M. Nieminen, *Phys. Rev. B* **34**, 3820 (1986).
- ³⁹Z. Q. Chen, S. J. Wang, M. Maekawa, A. Kawasuso, H. Naramolto, X. L. Yuan, and T. Sekiguchi, *Phys. Rev. B* **75**, 245206 (2007).
- ⁴⁰Z. Q. Chen, K. Betsuyaku, and A. Kawasuso, *Phys. Rev. B* **77**, 113204 (2008).
- ⁴¹Z. Q. Chen, M. Maekawa, A. Kawasuso, R. Suzuki, and T. Ohdaira, *Appl. Phys. Lett.* **87**, 091910 (2005).
- ⁴²Z. Q. Chen, S. Yamamoto, M. Maekawa, A. Kawasuso, and T. Sekiguchi, *J. Appl. Phys.* **94**, 4807 (2003).
- ⁴³F. Tuomisto, V. Ranki, K. Saarinen, and D C. Look, *Phys. Rev. Lett.* **91**, 205502 (2003).
- ⁴⁴X. L. Wang, Q. Shao, A. Zhuravlyova, M. He, Y. Yi, R. Lortz, J. N. Wang, and A. Ruotolo, *Sci. Rep.* **5**, 9221 (2015).
- ⁴⁵D. D. Wang, B. Zhao, N. Qi, Z. Q. Chen, and A. Kawasuso, *J. Mater. Sci.* **52**, 7067 (2017).
- ⁴⁶G. Rahman, V. M. García-Suárez, and S. C. Hong, *Phys. Rev. B* **78**, 184404 (2008).
- ⁴⁷X. Han, J. Lee, and H.-I. Yoo, *Phys. Rev. B* **79**, 100403(R) (2009).
- ⁴⁸J. Xu, Q. Li, W. Zhang, J. Liu, H. Du, and B. Ye, *Chem. Phys. Lett.* **616–617**, 161 (2014).
- ⁴⁹Y. Liu, G. Wang, S. Wang, J. Yang, L. Chen, X. Qin, B. Song, B. Wang, and X. Chen, *Phys. Rev. Lett.* **106**, 087205 (2011).
- ⁵⁰P. O. Lehtinen, A. S. Foster, Y. Ma, A. V. Krasheninnikov, and R. M. Nieminen, *Phys. Rev. Lett.* **93**, 187202 (2004).